Resting State Connectivity of the Human Habenula at Ultra-High Field

Salvatore Torrisi, Camilla L. Nord, Nicholas L. Balderston, Jonathan P. Roiser, Christian Grillon, Monique Ernst

PII: S1053-8119(16)30587-0
DOI: http://dx.doi.org/10.1016/j.neuroimage.2016.10.034
Reference: YNIMG13531

To appear in: *NeuroImage*

Received date: 26 August 2016
Accepted date: 20 October 2016

Cite this article as: Salvatore Torrisi, Camilla L. Nord, Nicholas L. Balderston Jonathan P. Roiser, Christian Grillon and Monique Ernst, Resting State Connectivity of the Human Habenula at Ultra-High Field, *NeuroImage* http://dx.doi.org/10.1016/j.neuroimage.2016.10.034

Resting State Connectivity of the Human Habenula at Ultra-High Field

Salvatore Torrisi[1], Camilla L. Nord[2], Nicholas L. Balderston[1], Jonathan P. Roiser[2], Christian Grillon[1], Monique Ernst[1]

Affiliations

[1] Section on the Neurobiology of Fear and Anxiety, National Institute of Mental Health, Bethesda, MD
[2] Neuroscience and Cognitive Neuropsychiatry group, University of College, London, UK

Abstract

The habenula, a portion of the epithalamus, is implicated in the pathophysiology of depression, anxiety and addiction disorders. Its small size and connection to other small regions prevent standard human imaging from delineating its structure and connectivity with confidence. Resting state functional connectivity is an established method for mapping connections across the brain from a seed region of interest. The present study takes advantage of 7 Tesla fMRI to map, for the first time, the habenula resting state network with very high spatial resolution in 32 healthy human participants. Results show novel functional connections in humans, including functional connectivity with the septum and bed nucleus of the stria terminalis (BNST). Results also show many habenula connections previously described only in animal research, such as with the nucleus basalis of Meynert, dorsal raphe, ventral tegmental area (VTA), and periaqueductal grey (PAG). Connectivity with caudate, thalamus and cortical regions such as the anterior cingulate, retrosplenial cortex and auditory cortex are also reported. This work, which demonstrates the power of ultra-high field for mapping human functional connections, is a valuable step toward elucidating subcortical and cortical regions of the habenula network.

Key words: 7 Tesla; anxiety; depression; seed-based functional connectivity

Introduction

The habenula is an evolutionarily-conserved brain structure important for emotion and reward modulation (Aizawa et al., 2011). It has attracted attention from researchers for its putative role in

negative affective states, including depression (Lawson et al., 2016), anxiety (Hikosaka, 2010), addiction (Velasquez et al., 2014), and pain (Shelton et al., 2012) . Because of its small size, however, it is difficult to examine this structure in humans. The current study is the first to address this limitation through the use of ultra-high resolution 7T imaging and resting state functional connectivity. The sensitivity of this approach makes it possible to build an accurate connectivity map of this structure. Such a map can provide a benchmark that permits comparison with animal work, drawing hypotheses about evolutionary changes across species, and a clearer understanding of putative functions of the habenula.

The habenula, a part of the epithalamus near the posterior commissure, is a connecting link among basal forebrain, striatal and midbrain regions (Hikosaka, 2010). It comprises a medial and a lateral portion with overlapping but distinct projections. Two afferent paths have been identified in the medial portion in rodents. One originates from septal nuclei and the nucleus basalis of Meynert via the stria medullaris. The second originates from the periaqueductal gray and raphe nuclei via the fasciculus retroflexus. The major efferent connections from the medial habenula project to much the same targets, as well as the lateral hypothalamus and ventral tegmental areas (Sutherland, 1982). The lateral habenula receives a number of forebrain afferents, including the diagonal band of Broca, globus pallidus and hypothalamus, and projects to multiple regions including the rostromedial tegmental nucleus (RMTg), ventral tegmental area, ventral striatum, substantia inominata, dorsomedial nucleus of the thalamus, raphe nuclei and periaqueductal gray (Sutherland, 1982).

The aforementioned subcortical connectivity is consistent with the notion that the habenula plays a role in multiple processes, including reward and stress (Hikosaka, 2010). For example, single cell recording studies in rodents and primates reveal that the lateral habenula responds to prediction error and negative reward (Pobbe and Zangrossi, 2008; Proulx et al., 2014). Likewise, the lateral habenula's connection with the raphe nuclei suggests a role of this structure in modulating the serotoninergic system (Roiser et al., 2009; Shabel et al., 2012; Zhao et al., 2015).

Due to its influence on monoaminergic systems, the habenula has been implicated in two major classes of psychiatric disorders: depression and anxiety. Indirect evidence for the role of the habenula in

depression comes from studies that implicate this structure in models of learned helplessness in animals (Gass et al., 2014; Mirrione, 2014), and during encoding of negative motivational values in humans (Lawson et al., 2014). Recent work in humans has demonstrated abnormal habenula responses during primary aversive conditioning in depression (Lawson et al., 2016), strengthening a previous case report describing remission from intractable depression following deep brain stimulation of the habenula (Sartorius et al., 2010). Anatomically, the habenula has also been found to be larger in individuals with more severe depression (Schmidt et al., 2016). Evidence from animal research suggests that the habenula is an important component of stress and anxiety circuits as well (Mathuru and Jesuthasan, 2013; Pobbe and Zangrossi, 2008; Viswanath et al., 2013; Yamaguchi et al., 2013).

Collectively, these data highlight the potential importance of the habenula in psychopathology, but this notion requires a better understanding of its functional circuitry. One strategy to address this question in humans is through the functional connectivity of endogenous, low-frequency fluctuations of fMRI blood-oxygen-level dependent (BOLD) signal, an established method of mapping functional networks (Fox and Raichle, 2007). Other researchers have already begun mapping the habenula network in this manner, using standard 3T field strength, which suffers from limited signal to noise ratio. These studies have revealed a number of connections. For example, one study reported resting state habenula connectivity with the ventral tegmental area (VTA), thalamus and sensorimotor cortex, as well as connectivity differences between subjects with low versus high subclinical depression (Ely et al., 2016). Another study acquired cardiac-gated functional images, revealing connectivity to subcortical areas such as the VTA and periaqueductal grey (PAG) (Hétu et al., 2016). The authors of these studies suggest that some of these findings should be considered with caution, particularly considering the small size of the habenula and some of its identified targets. Nonetheless, these studies represent an important starting point for the evaluation of habenula connectivity in humans, which can be more clearly identified using ultra-high field fMRI.

Ultra-high field (≥7 Tesla [7T]) fMRI has a greatly improved BOLD signal-to-noise ratio compared to 3T scanners (van der Zwaag et al., 2009), and enables the acquisition of finer spatial

resolution. As with our previous study of the bed nucleus of the stria terminalis (BNST) at 7T (Torrisi et al., 2015), we hypothesized that we would recover much of the habenula functional network known from animal studies, and further uncover connectivity unique to humans. These mappings will pave the way for more targeted testing of habenula function by using cognitive and emotional tasks.

Materials and Methods

Subjects

Thirty-four right-handed, healthy volunteers from a mixed urban and suburban population were recruited through internet advertisements, flyers, and print advertisements, and were compensated for their time. This sample was an extension of a previous study (Torrisi et al., 2015). Exclusion criteria included: (a) current or past Axis I psychiatric disorder as assessed by SCID-I/NP (First et al., 2007), (b) first degree relative with a known psychotic disorder, (c) brain abnormality on MRI as assessed by a radiologist, (**d**) positive toxicology screen, (**e**) MRI contraindication, or (**f**) excessive head motion during the functional scans. Depressive symptoms were assessed with the Beck Depression Inventory (Beck et al., 1961). Excessive head motion was defined as more than 15% of a subject's images censored, where the criterion for censoring was a Euclidean norm motion derivative greater than 0.3mm for temporally adjacent time points. Two subjects were removed for this reason, yielding an N=32 for the study (16 females, mean (SD) age = 27.57 (5.8)). Subjects showed no evidence of depressive symptoms (mean (SD) Beck Depression Inventory scores = 0.9 (1.3)). Written informed consent was obtained from subjects, approved by the National Institute of Mental Health (NIMH) Combined Neuroscience Institutional Review Board.

Functional image acquisition

Data acquisition was identical to our previous work on the BNST (Torrisi et al., 2015) and is described here briefly. Images were acquired on a 7T Siemens Magnetom MRI with a 32-channel head coil. Third-order shimming was implemented to correct for magnetic inhomogeneities (Pan et al., 2011).

We collected a high-resolution, 0.7mm isotropic, T1-weighted MPRAGE anatomical image. The functional images had 1.3mm isotropic voxels, an interleaved TR of 2.5 seconds, and 240 images collected over a 10-minute acquisition. Our EPI field of view (FOV) covered ~2/3 of the brain (supplemental Figure 1). Participants were instructed to keep their eyes open and look at a white fixation cross on a black background.

Physiological measures

To clean the fMRI data for physiological signals of non-interest, respiration was measured with a pneumatic belt placed around the stomach and cardiac rhythm with a pulse oximeter around the index finger. Data were sampled at 500hz using a BioPac MP150 system (www.biopac.com).

Habenula definition

One rater (author CN) separately drew left and right habenulae on the subjects' anatomical images in AC-PC-aligned native space, as outlined in a validated protocol (Lawson et al., 2013). The drawing process, performed in AFNI (Cox, 1996), was also informed by verifying anatomical landmarks using a detailed atlas (Mai et al., 2015). Briefly, the protocol involved distinguishing the habenula from adjacent cerebral spinal fluid, posterior commissure, medial thalamus and stria medullaris. Following manual tracing of the habenula, the volumes of the left and right habenulae for each subject were computed separately. Because of reports of structural and functional laterality differences (Ahumada-Galleguillos et al., 2016; Bianco and Wilson, 2009; Hétu et al., 2016), left and right habenula volumes were compared using a paired t-test.

Preprocessing

Preprocessing and analysis proceeded identically to our previous work with the BNST (Torrisi et al., 2015) and is described briefly. Tissues were segmented for each individual with FreeSurfer (Fischl et al., 2002). Resting state preprocessing and analyses were then performed within AFNI. Subjects' first three functional volumes were removed to allow for scanner equilibrium and the remaining functional

volumes were slice-time and motion corrected, and coregistered to their structural image. Subjects' anatomy was non-linearly normalized to a skull-stripped *ICBM 2009b Nonlinear Asymmetric* template in MNI space using *3dQwarp* (Cox and Glen, 2013). The resulting transformation parameters were then applied to the hand-drawn habenulae, FreeSurfer segmentations and functional data. A group average of the normalized habenulae was created to check alignment (supplemental Figure 2). Functional images were smoothed with a 2.6 mm FWHM Gaussian kernel.

A number of time series were then modeled as covariates of non-interest and regressed out to leave residuals with which voxel-wise correlations were performed. Regressors of no interest included: 0.01-0.1 hz bandpass filter regressors; 6 head motion parameters and their 6 derivatives; 13 slice-based cardiac (RETROICOR) and respiration volume per unit time (RVT) measures (Birn et al., 2008; Glover et al., 2000) and two time series from lateral and 3^{rd}+4^{th} ventricle masks. Finally, the regressions were performed at each gray matter voxel within a 13mm radius sphere which took into account local white matter (ANATICOR method), which controls for both signal heterogeneity and hardware-related artifacts (Jo et al., 2010).

The residual maps after these regressions contained the BOLD signals of interest and were used to extract a mean time series from the combined left and right habenula masks. Paired t-tests additionally looked for lateralization of functional connectivity across the brain. The combined masks were used after finding a lack of significant differences between right and left habenula connectivity when computed separately. This time series was correlated across the rest of the brain within a mask that represented the EPI coverage of 95% or more of the 32 subjects. Finally, correlations were Fisher-transformed and entered into a one-sample t-test.

The resulting maps were thresholded at ($p=1x10^{-7}$), k=5, because anything more conservative than $p=1x10^{-5}$ was not amenable to cluster correction using *3dClustSim*. This more stringent threshold was used because correcting at the strictest calculable correction with the cluster-based approach, while using an updated spatial autocorrelation function (Cox et al., 2016), still produced maps with large clusters encompassing several regions, thus compromising anatomical specificity. Note that a cluster size

of k=10 was used for Table 1, while the full table (k=5) is presented in the supplemental materials. All clusters survive whole-brain correction for multiple comparisons.

Results

Habenula volume

The mean (SD) volume was 18.8 (6.0) mm^3 for the left habenula, and 14.9 (4.0) mm^3 for the right habenula. A two-tailed, paired t-test demonstrated that this difference in volume (left habenula larger than right) was significant ($t(31)=4.5$; $p=0.000093$). Females did not differ from males on left ($t(30)=0.05$; $p=0.96$) or right ($t(30)=0.8$; $p=0.44$) habenula volume with a two-sample t-test.

Habenula functional connectivity

The pattern of habenula functional connectivity was very similar to the anatomical connectivity reported in other vertebrates and non-human primates. In addition, connectivity was observed with specific cortical regions that have not been reported in the animal literature. The findings are summarized as Figures 1-3, Table 1, Supplementary Table 1 and discussed below.

The thalamus showed the highest degree of functional connectivity (Figure 1) - it was the most prominent portion of a large cluster that spread anteriorly from the habenula. The other subcortical regions functionally connected with the habenula included three major areas: (1) striatal regions such as the putamen and head of the caudate (Figure 2A), (2) limbic and basal forebrain structures such as the BNST, nucleus basalis of Meynert (CH4 subregion; (Zaborszky et al., 2008)), posterior hippocampus and septal nuclei (Figures 2A-C) and (3) midbrain/brainstem structures such as the periaqueductal gray, dorsal raphe nuclei and ventral tegmental area (Figures 2D, E, F). Notably, the dorsal raphe cluster appears to correspond to the serotonergic R2 region (Son et al., 2014; 2012). Also reported in Table 1 are connections with the parahippocampal gyrus and dorsal cerebellum.

Additionally, the habenula exhibited strong functional connectivity with cortical regions such as

the dorsal anterior cingulate cortex / medial prefrontal cortex, left inferior frontal sulcus, and the middle and posterior anterior cingulate (arrows in Figure 3A). The habenula was also functionally connected with the retrosplenial cortex (Figure 3B), primary visual cortex (Figure 1), primary auditory cortex, i.e. Heschl's gyrus (Morosan et al., 2001) and posterior insula (Figure 3C).

There was no difference between left and right habenula functional connectivity at the selected statistical threshold, as well as no difference when the threshold was relaxed to $p=1x10^{-5}$ but still whole-brain corrected.

Discussion

The objective of this first ultra-high field resting state fMRI study of the habenula was to examine, in detail, its coupling with cortical and small subcortical regions. Our findings, together with knowledge from animal work, help to inform the various roles of the habenula in humans, and guide future research on the contribution of this structure to adaptive and maladaptive behaviors.

The current study replicates and extends findings from previous resting state studies, optimizing anatomical specificity and statistical significance. Therefore, the present findings could serve as a standard of the habenula functional connectivity at rest that could inform other works using less advanced instrumentation. A handful of recent studies have examined habenula resting state functional connectivity using standard 3-Tesla scanners (Ely et al., 2016; Erpelding et al., 2014; Hétu et al., 2016) while enhancing acquisition parameters to optimize spatial resolution (see in particular Hétu et al., although at the expense of field-of-view). Present findings replicate the habenula coupling with the relatively large regions of these previous reports; however, we also reveal connectivity previously only observed in animal work. In particular, the study identifies functional coupling between the habenula and small subcortical structures that cannot be reliably captured with standard fMRI. Present findings also fail to replicate a subset of previous findings, while others have never been reported. These three types of findings (replicated, unreplicated, and novel) are discussed below.

Replicated findings

Replicated findings include both cortical and subcortical connectivity. Cortically, the habenula is functionally coupled with the medial prefrontal cortex, cingulate cortex (anterior through posterior), parieto-occipital cortex, retrosplenial cortex, and posterior insula. **Diffusion-weighted tractography in humans has shown fibers running anterior and dorsally from the habenula, which may connect to these regions (figure 9 of (Strotmann et al., 2014)).** Subcortically, the habenula is functionally coupled with thalamus, hippocampus, parahippocampus, septofimbria nucleus, and striatum (caudate and putamen). **Strong structural connections throughout the thalamus, for example, has been shown using probabilistic diffusion tractography of the habenula (figure 8 of (Strotmann et al., 2014)). These authors were able to additionally confirm the presence of the stria medullaris connecting the habenula with forebrain regions and the fasciculus retroflexus descending ventrally into the midbrain.** In addition, the habenula showed connectivity with the major cholinergic nucleus, the nucleus basalis de Meynert, the dopaminergic VTA, the PAG, and the serotonergic dorsal raphe nuclei. Connectivity between the habenula and the cerebellum was also detected. Collectively, these findings raise two points. First, they attest to the high degree of evolutionary conservation of the subcortical connectivity of the habenula. Second, they suggest a central role of the habenula in emotional / motivational brain circuitry.

Animal work through tract-tracing and lesion studies has identified the major afferent and efferent projections of the habenula, which parallel the human functional connectivity reported here (Herkenham and Nauta, 1977; Sutherland, 1982). As such, the habenula may possibly play a critical role in survival, and thus in adaptive behavior. In fact, its connectivity pattern suggests that it may function as a link between the forebrain and midbrain during emotional and motivational processing. Specifically, the forebrain structures that are coupled with the habenula are strongly implicated in emotion/motivation processing for both aversive (e.g., hippocampus, insula, anterior cingulate cortex) (Hayes and Northoff, 2012), and appetitive (e.g., striatum) (Hardin et al., 2009) information. The midbrain structures coupled

with the habenula include dopaminergic, serotonergic and cholinergic nuclei, which provide important modulatory input to a wide variety of brain structures. Therefore, the forebrain-midbrain link provided by the habenula may play an important role in establishing and maintaining emotional/motivational states.

The habenula has recently received a surge of interest in relation to its potential role in psychopathology, particularly depression (Lawson et al., 2016) and anxiety (Hikosaka, 2010), but also addiction (Velasquez et al., 2014) and chronic pain (Shelton et al., 2012). The habenula might contribute to depressive symptoms by failing to activate serotonergic nuclei (Roiser et al., 2009; Zhao et al., 2015), or by excessively activating inhibitory cells that synapse on VTA dopamine neurons (Balcita-Pedicino et al., 2011). These effects could potentially contribute to the cardinal depressive symptom of anhedonia. Regarding addiction, the habenula has been implicated in addictive behavior based on its strong influence on dopamine activity within the reward system (i.e., VTA/striatum) and its sensitivity to negative prediction error (i.e., activated by unpredicted unfavorable feedback) (Matsumoto and Hikosaka, 2007).

Unreplicated findings

In some cases, we did not replicate findings from previous studies of human habenula connectivity. Previously, the norepinephrine system has been implicated in the role of the habenula in stress responses (e.g., Velasquez et al. 2014), and one human resting state study using 3T reports connectivity with the locus coeruleus (Erpelding et al., 2014). In the present study, this connection was not detected, **perhaps because noise cleaning and statistical thresholding differed significantly from Erpelding et al's work.** Currently, animal studies have not been consistent in demonstrating habenula-locus coeruleus projections (e.g., Hikosaka 2010, Herkenham 1979). **Another inconsistency with human studies (Ely et al., 2016; Erpelding et al., 2014; Lawson et al., 2014) concerns the amygdala. In contrast to these studies, the present work fails to identify habenula-amygdala functional connectivity. This lack of connectivity is actually consistent with rodent findings, showing an absence of afferent and efferent connections between both structures (Herkenham and Nauta, 1977; Quina et al., 2015). In the context of human fMRI this** inconsistency may have occurred due to a Type

1 error in the previous studies, or a Type 2 error herein. An important question is whether both couplings with locus coeruleus or amygdala would be particularly activated in stressful conditions.

Previously, laterality differences in functional connectivity have also been reported (Hétu et al., 2016). In our study, we observed no significant differences between right and left habenula functional connectivity **(see supplemental figures S4 and S5 for separate connectivity maps of left and right habenula).** However, a significant volumetric difference was found, with the left habenula larger than the right, which replicates previous volumetric findings in humans (Ahumada-Galleguillos et al., 2016). One notes that this anatomical difference does not necessarily imply functional lateralization. Therefore, it is too early to speculate on the functional significance of human habenula lateralization despite preliminary findings in humans (Hétu et al., 2016) and animals (Dreosti et al., 2014). Finally, the lateral hypothalamus, known from animal studies to receive habenula projections **(Quina et al., 2015)**, was also not detected. **This is consistent with other human resting state studies (Ely et al., 2016; Erpelding et al., 2014; Hétu et al., 2016). The lateral hypothalamus is a very small structure rarely reported in human fMRI research and is perhaps even too small for our spatial resolution. Furthermore, the lateral hypothalamus is an output physiological effector region that may not be strongly recruited at rest.**

Novel findings

Previous studies in humans have not reported functional connectivity with the septal nuclei or BNST. The finding of connectivity with the septal nuclei (figure 2C) is particularly interesting given their role in regulating processes related to mood, motivation and neuropsychiatric disorders (Sheehan et al., 2004). Habenula coupling was also detected with the BNST (figure 2A), an extended amygdalar region strongly implicated in fear and anxiety (Davis et al., 2010). This habenula-BNST connectivity echoes the finding in our previous study, in which habenula connectivity was observed using a BNST seed (Torrisi et al., 2015). Interestingly, in one study (Gass et al., 2014), the BNST showed an inverse resting metabolic relationship (regional cerebral blood volume) with the habenula in a rodent model of congenital learned

helplessness. The authors speculated that functional alterations in both structures might mediate learning associated with stress, or may reflect vulnerability after chronic stress to depression. The direct coupling of these two structures may also relate to the frequent comorbidity of depression and anxiety (Hirschfield, 2001), although further work is necessary to establish this link.

Finally, a novel finding relative to both human and animal studies concerns the strong functional connectivity between the habenula and Heschl's gyrus, the primary auditory cortex. Although connectivity with other primary visual (here) and sensorimotor (Ely et al., 2016) areas have been reported with the habenula, our study is the first to show its coupling with a region most implicated in auditory processing. **Because the habenula is so evolutionarily conserved across species, any early connections with primary sensory cortices may have been phylogenetically conserved as well.** Nonetheless it is premature to speculate on the significance of this **connection in relation to traditional habenula functioning,** and future work should **replicate the existence of and** investigate the functional relevance of this finding.

Limitations

One general caveat of any fMRI-based functional connectivity study is the implicit assumption that a strongly thresholded connectivity map reflects underlying anatomical connectivity. This is not necessarily true: anatomical structure is thought to constrain but not determine function (Stephan et al., 2009). The results presented here may therefore be functionally mediated by other regions and, in some cases, the identified structures will not be connected with the habenula monosynaptically. The relationship between functional and structural connectivity is still under investigation (Honey et al., 2010; Ng et al., 2013). Further work is needed with animals, computational models, and testing the effects of surgical interventions (Johnston et al., 2008). The results presented here are nonetheless compelling in how strongly they parallel known anatomical connectivity.

Another limitation is that two regions known to be anatomically connected with the habenula, the

substantia nigra and globus pallidus (Hikosaka, 2010), were not recovered at ultra-high field. The reason is that these areas of the brain accumulate iron throughout the lifespan (Hallgren and Sourander, 1958), and, with T2*-based sequences, iron-related signal dropout is more pronounced at higher fields (Peters et al., 2007). Therefore, the null finding in relation to habenula functional connectivity with these regions is likely explained by this phenomenon (supplemental Figure 3). Furthermore, our incomplete brain coverage, determined from a common temporal/spatial trade-off, prevented us from detecting connectivity with superior cortical regions, such as the sensorimotor cortex, which has previously been observed to functionally connect with the habenula (Ely et al., 2016). **In addition, although we acquired data with high spatial resolution, lateral and medial habenula subdivisions could not be distinguished, in contrast to recent in vivo and ex vivo studies at 7T of habenula structure (Strotmann et al., 2014; 2013). Therefore, this inability** to resolve medial and lateral subdivisions of the habenula **means that** our results likely reflect connectivity with both subdivisions.

Finally, we selected a stringent statistical threshold based on several factors, including the general spatial extents of the regions known to connect with the habenula, the consequences of preprocessing on spatial specificity (registration and smoothing), and the need to report a reasonably-sized table of coordinates for meta-analyses and ROI definitions (Table 1). Although such an approach increases the probability of type II error (false negatives) in the final statistical maps, it also increases confidence in the results that are reported.

Conclusion

The present findings provide the strongest information to date on the resting functional connectivity of the habenula complex in humans, made possible with the use of ultra-high field imaging. Taken together, these results place the habenula, functionally, at the intersection of the forebrain and midbrain, acting as a relay among dopaminergic, serotonergic and cholinergic neurotransmitter systems. In view of this central position from both an anatomical and functional perspective, the habenula is likely to play a critical role in adaptive behaviors, maintaining and adjusting a balance among centers of

emotion and behavioral outputs. In fact, the habenula has been strongly implicated in depression, anxiety and addiction. Now that this small structure can be more accurately defined with ultra-high field imaging in humans, the present study will hopefully represent the continuation of a rich road leading to discoveries that will foster new understanding and treatments of psychopathology.

Acknowledgments: Special thanks to Rick Reynolds and Daniel Glen for analysis help, Katherine O'Connell, Andrew Davis, Gaby Alvarez and Joseph Leshin for data collection help, Bari Fuchs for generating the anatomical underlay, Erika Raven for iron deposition insight, and Okihide Hikosaka for valuable feedback. This work utilized the computational resources of the NIH HPC Biowulf cluster (http://hpc.nih.gov). This work was supported by the Intramural Research Program of the National Institutes of Mental Health, project number ZIAMH002798 (clinical protocol 02-M-0321, NCT00047853) to CG. JPR is a consultant for Cambridge Cognition, though this is not relevant to the current work. The authors report no competing interest. The author(s) declare that, except for income received from the primary employer, no financial support or compensation has been received from any individual or corporate entity over the past 3 years for research or professional service and there are no personal financial holdings that could be perceived as constituting a potential conflict of interest.

Figures Captions & Table

Figure 1. Whole brain (within field of view) results in axial slices, overlaid on averaged group anatomy that had been nonlinearly normalized to an MNI template. $p<0.0000001$. Left is left. The same thresholding and color scale are used for Figures 2 and 3. Note that the large epi/thalamus cluster does not include the lateral geniculate nucleus, medial geniculate nucleus, lateral pulvinar and anterior lateral nuclei.

Figure 2. A–F: Habenula functional connectivity with subcortical regions, magnified views. Overlaid on MNI2009a template.

Figure 3. A–C: Habenula functional connectivity with cortical regions. Arrows (left to right) point to A: supragenual anterior cingulate cortex (ACC), dorsal ACC and posterior ACC. B: retrosplenial cortex. C: left primary auditory cortex and posterior insula.

REGION	X	Y	Z	cluster size	peak tstat
LEFT HEMISPHERE					
subcortical					

bed nucleus of the stria terminalis (BNST)	-3.7	3.1	-3.8	10	9.15
nucleus basalis of meynert (CH4) / piriform cortex	-25.8	1.8	-11.5	137	11.95
caudate	-15.4	3.1	15.8	22	8.15
caudate	-15.4	-0.9	18.3	11	7.65
caudate	-31	8.2	-3.8	14	8.83
putamen tail	-29.7	-6.1	-9	35	8.85
bilateral habenulae, epithalamus and thalamus	-5	-23	2.8	5,010	24.93
hippocampus (FD)	-27.1	-25.6	-14.2	16	8.44
anterior thalamus (prefrontal)	-10.2	-7.3	9.2	10	8.56
periaqueductal gray	-3.7	-30.8	-7.7	18	8.93
cerebellum lobule V	-2.4	-52.8	-1.2	11	8.35
cortical					
frontal superior gyrus (BA 10)	-1.1	52.4	10.5	37	9.06
frontal superior gyrus /MFG (BA 32)	-3.7	38.1	27.4	27	9.95
inferior frontal sulcus (BA 45)	-44	31.6	17	12	9.3
insula inferior circular sulcus (BA 13)	-38.8	-2.2	-7.7	12	8.16
insula posterior / OP 2 (BA 13)	-38.8	-19.1	19.7	16	8.14
superior temporal Heschl gyrus / TE 1.0 (BA 41)	-45.2	-21.7	11.8	113	12.99
transverse temporal sulcus / TE 1.1 (BA 22)	-42.7	-24.2	2.8	38	10.65
cingulate posterior-dorsal (BA 23)	-5	-46.3	23.5	79	9.17
cingulate middle posterior (BA 24)	-6.2	-3.4	39.1	10	9.73
cingulate middle posterior (BA 24)	-3.7	-8.7	37.8	10	8.56
cingulate middle anterior (BA 24)	-2.4	18.6	28.8	17	8.37
cingulate middle posterior	-2.4	-13.8	32.7	14	7.99
calcarine sulcus / lingual gyrus (BA 17)	-19.2	-55.4	2.8	29	8.33
calcarine sulcus (BA 17)	-18	-67.2	4	12	9.21
calcarine sulcus (BA 17)	-10.2	-76.2	11.8	19	8.4
calcarine sulcus / V1 (BA 17)	-8.9	-80.1	5.3	87	9.19
RIGHT HEMISPHERE					
subcortical					
nucleus basalis of meynert (CH4) / piriform cortex	23.6	1.8	-11.5	167	10.74
septofimbrial nucleus	2.8	-2.2	10.5	11	8.55
caudate	10.6	8.2	11.8	13	8.69
caudate	14.5	17.3	-5.1	15	9.18
parahippocampal gyrus	22.3	-28.2	-6.3	12	7.99
posterior hippocampus FD	28.8	-32.1	-9	33	9.34
cerebellum lobule V	6.8	-55.4	-7.7	22	8.75
cortical					
front superior gyrus (BA 8)	1.5	31.6	41.8	47	9.75
cingulate anterior (BA 32)	0.2	43.3	15.8	168	11.67

cingulate anterior (BA 32)	9.3	39.4	19.7	11	8.04
cingulate anterior (BA 32)	10.6	35.6	23.5	36	9.39
cingulate middle anterior (BA 32)	5.4	29.1	28.8	74	9.45
cingulate middle anterior (BA 32)	1.5	17.3	40.4	156	9.72
cingulate middle posterior (BA 23)	2.8	-19.1	35.2	20	7.67
cingulate posterior (BA 23)	2.8	-30.8	28.8	222	9.28
pericallosal / retrosplenial sulcus (BA 29)	9.3	-45.1	10.5	111	9.63
parieto-occipital sulcus / precuneus (BA 18)	10.6	-65.8	26.2	10	7.81
parieto-occipital sulcus / precuneus	19.7	-61.9	23.5	26	7.93
parieto-occipital sulcus	17.1	-52.8	18.3	11	7.89
calcarine sulcus (BA 18)	18.4	-43.8	-5.1	14	9.15

Table 1. Peak clusters are organized first by hemisphere, then whether they are subcortical or cortical (horizontal lines separate subcortical from cortical) and then roughly from rostral to caudal. Indentation distinguishes sub-clusters. Brodmann areas (BA) are reported for general orientation. Labeling chosen from the higher probability of two atlases (Destrieux et al., 2010; Eickhoff et al., 2005). Clusters are thresholded at $p<0.0000001$, $k=10$; see Supplemental Table 1 for full $k=5$ cluster list. Coordinates are in MNI space, but also more specifically correspond to the template used.

References

Ahumada-Galleguillos, P., Lemus, C.G., Díaz, E., Osorio-Reich, M., Härtel, S., Concha, M.L., 2016. Directional asymmetry in the volume of the human habenula. Brain Struct Funct 1–6. doi:10.1007/s00429-016-1231-z

Aizawa, H., Amo, R., Okamoto, H., 2011. Phylogeny and Ontogeny of the Habenular Structure. Frontiers in Neuroscience 5. doi:10.3389/fnins.2011.00138

Balcita-Pedicino, J.J., Omelchenko, N., Bell, R., Sesack, S.R., 2011. The inhibitory influence of the lateral habenula on midbrain dopamine cells: Ultrastructural evidence for indirect mediation via the rostromedial mesopontine tegmental nucleus. The Journal of Comparative Neurology 519, 1143–1164. doi:10.1002/cne.22561

Beck, A.T., Ward, C.H., Mendelson, M., Mock, J., Erbaugh, J., 1961. An Inventory for Measuring Depression. Archives of General Psychiatry 561–571.

Bianco, I.H., Wilson, S.W., 2009. The habenular nuclei: a conserved asymmetric relay station in the vertebrate brain. Philosophical Transactions of the Royal Society B: Biological Sciences 364, 1005–1020. doi:10.1098/rstb.2008.0213

Birn, R.M., Smith, M.A., Jones, T.B., Bandettini, P.A., 2008. The respiration response function: The temporal dynamics of fMRI signal fluctuations related to changes in respiration. NeuroImage 40, 644–654. doi:10.1016/j.neuroimage.2007.11.059

Cox, R.W., 1996. AFNI: software for analysis and visualization of functional magnetic resonance neuroimages. Comput. Biomed. Res. 29, 162–173.

Cox, R.W., Glen, D.R., 2013. Nonlinear Warping in AFNI. Poster presented at the 19th Annual Meeting of the Organization for Human Brain Mapping, Seattle, WA, USA.

Cox, R.W., Reynolds, R.C., Taylor, P.A., 2016. AFNI and Clustering: False Positive Rates Redux. bioRxiv 1–15. doi:10.1101/065862

Davis, M., Walker, D.L., Miles, L., Grillon, C., 2010. Phasic vs Sustained Fear in Rats and Humans: Role of the Extended Amygdala in Fear vs Anxiety. Neuropsychopharmacology 35, 105–135. doi:10.1038/npp.2009.109

Destrieux, C., Fischl, B., Dale, A., Halgren, E., 2010. Automatic parcellation of human cortical gyri and sulci using standard anatomical nomenclature. NeuroImage 53, 1–15. doi:10.1016/j.neuroimage.2010.06.010

Dreosti, E., Llopis, N.V., Carl, M., Yaksi, E., Wilson, S.W., 2014. Left-Right Asymmetry Is Required for the Habenulae to Respond to Both Visual and Olfactory Stimuli. Current Biology 24, 440–445. doi:10.1016/j.cub.2014.01.016

Eickhoff, S.B., Stephan, K.E., Mohlberg, H., Grefkes, C., Fink, G.R., Amunts, K., Zilles, K., 2005. A new SPM toolbox for combining probabilistic cytoarchitectonic maps and functional imaging data. NeuroImage 25, 1325–1335. doi:10.1016/j.neuroimage.2004.12.034

Ely, B.A., Xu, J., Goodman, W.K., Lapidus, K.A., Gabbay, V., Stern, E.R., 2016. Resting-state functional connectivity of the human habenula in healthy individuals: Associations with subclinical depression. Hum. Brain Mapp. doi:10.1002/hbm.23179

Erpelding, N., Sava, S., Simons, L.E., Lebel, A., Serrano, P., Becerra, L., Borsook, D., 2014. Habenula functional resting-state connectivity in pediatric CRPS. Journal of Neurophysiology 111, 239–247. doi:10.1152/jn.00405.2013

First, M.B., Spitzer, R.L., Gibbon, M., Williams, J., 2007. Structured Clinical Interview for DSM-IV-TR Axis I Disorders – Non-Patient Edition (SCID-I/NP, 1/2007 Revision).

Fischl, B., Salat, D.H., Busa, E., Albert, M., Dieterich, M., Haselgrove, C., van der Kouwe, A., Killiany, R., Kennedy, D., Klaveness, S., 2002. Whole brain segmentation: automated labeling of neuroanatomical structures in the human brain. Neuron 33, 341–355.

Fox, M.D., Raichle, M.E., 2007. Spontaneous fluctuations in brain activity observed with functional magnetic resonance imaging. Nat Rev Neurosci 8, 700–711. doi:10.1038/nrn2201

Gass, N., Cleppien, D., Zheng, L., Schwarz, A.J., Meyer-Lindenberg, A., Vollmayr, B., Weber-Fahr, W., Sartorius, A., 2014. Functionally altered neurocircuits in a rat model of treatment-resistant depression show prominent role of the habenula. European Neuropsychopharmacology 24, 381–390. doi:10.1016/j.euroneuro.2013.12.004

Glover, G.H., Li, T.Q., Ress, D., 2000. Image-based method for retrospective correction of physiological motion effects in fMRI: RETROICOR. Magn Reson Med 44, 162–167.

Hallgren, B., Sourander, P., 1958. The Effect of Age on the Non-Haemin Iron in the Human Brain. Journal of Neurochemistry 3, 41–51.

Hardin, M.G., Pine, D.S., Ernst, M., 2009. The influence of context valence in the neural coding of monetary outcomes. NeuroImage 48, 249–257. doi:10.1016/j.neuroimage.2009.06.050

Hayes, D.J., Northoff, G., 2012. Common brain activations for painful and non-painful aversive stimuli. BMC Neurosci 13, 60. doi:10.1186/1471-2202-13-60

Herkenham, M., Nauta, W.J., 1977. Afferent connections of the habenular nuclei in the rat. A horseradish peroxidase study, with a note on the fiber-of-passage problem. The Journal of Comparative Neurology 173, 123–146. doi:10.1002/cne.901730107

Hétu, S., Luo, Y., Saez, I., D'Ardenne, K., Lohrenz, T., Montague, P.R., 2016. Asymmetry in functional connectivity of the human habenula revealed by high-resolution cardiac-gated resting state imaging. Hum. Brain Mapp. doi:10.1002/hbm.23194

Hikosaka, O., 2010. The habenula: from stress evasion to value-based decision-making. Nat Rev Neurosci 11, 503–513. doi:10.1038/nrn2866

Hirschfield, R.M.A., 2001. The Comorbidity of Major Depression and Anxiety Disorders. Prim. Care Companion J. Clin. Psychiatry 03, 244–254. doi:10.4088/PCC.v03n0609

Honey, C.J., Thivierge, J.-P., Sporns, O., 2010. Can structure predict function in the human brain? NeuroImage 52, 766–776. doi:10.1016/j.neuroimage.2010.01.071

Jo, H.J., Saad, Z.S., Simmons, W.K., Milbury, L.A., Cox, R.W., 2010. Mapping sources of correlation in resting state FMRI, with artifact detection and removal. NeuroImage 52, 571–582.

doi:10.1016/j.neuroimage.2010.04.246
Johnston, J.M., Vaishnavi, N.S., Smyth, M.D., Zhang, D., He, B.J., Zempel, J.M., Shimony, J.S., Snyder, A.Z., Raichle, M.E., 2008. Loss of Resting Interhemispheric Functional Connectivity after Complete Section of the Corpus Callosum. The Journal of Neuroscience 28, 6453–6458. doi:10.1523/JNEUROSCI.0573-08.2008
Lawson, R.P., Drevets, W.C., Roiser, J.P., 2013. Defining the habenula in human neuroimaging studies. NeuroImage 64, 722–727. doi:10.1016/j.neuroimage.2012.08.076
Lawson, R.P., Nord, C.L., Seymour, B., Thomas, D.L., Dayan, P., Pilling, S., Roiser, J.P., 2016. Disrupted habenula function in major depression. Mol Psychiatry 1–7. doi:10.1038/mp.2016.81
Lawson, R.P., Seymour, B., Loh, E., Lutti, A., Dolan, R.J., Dayan, P., Weiskopf, N., Roiser, J.P., 2014. The habenula encodes negative motivational value associated with primary punishment in humans. Proceedings of the National Academy of Sciences 111, 11858–11863. doi:10.1073/pnas.1323586111
Mai, J.K., Majtanik, M., Paxinos, G., 2015. Atlas of the human brain, 4 ed. Academic Press.
Mathuru, A.S., Jesuthasan, S., 2013. The medial habenula as a regulator of anxiety in adult zebrafish. Frontiers in Neural Circuits 7, 1–3. doi:10.3389/fncir.2013.00099/full
Matsumoto, M., Hikosaka, O., 2007. Lateral habenula as a source of negative reward signals in dopamine neurons. Nature 447, 1111–1115. doi:10.1038/nature05860
Mirrione, M.M., 2014. Increased metabolic activity in the septum and habenula during stress is linked to subsequent expression of learned helplessness behavior. Frontiers in Human Neuroscience 8, 1–8. doi:10.3389/fnhum.2014.00029/abstract
Morosan, P., Rademacher, J., Schleicher, A., Amunts, K., Schormann, T., Zilles, K., 2001. Human Primary Auditory Cortex: Cytoarchitectonic Subdivisions and Mapping into a Spatial Reference System. NeuroImage 13, 684–701. doi:10.1006/nimg.2000.0715
Ng, B., Varoquaux, G., Poline, J.-B.P., Thirion, B., 2013. Implications of inconsistencies between fMRI and dMRI on multimodal connectivity estimation. Med Image Comput Comput Assist Interv 16, 652–659.
Pan, J.W., Lo, K.-M., Hetherington, H.P., 2011. Role of very high order and degree B0 shimming for spectroscopic imaging of the human brain at 7 tesla. Magnetic Resonance Medicine 68, 1007–1017. doi:10.1002/mrm.24122
Peters, A.M., Brookes, M.J., Hoogenraad, F.G., Gowland, P.A., Francis, S.T., Morris, P.G., Bowtell, R., 2007. T2* measurements in human brain at 1.5, 3 and 7 T. Magnetic Resonance Imaging 25, 748–753. doi:10.1016/j.mri.2007.02.014
Pobbe, R.L.H., Zangrossi, H., Jr., 2008. Involvement of the lateral habenula in the regulation of generalized anxiety- and panic-related defensive responses in rats. Life Sciences 82, 1256–1261. doi:10.1016/j.lfs.2008.04.012
Proulx, C.D., Hikosaka, O., Malinow, R., 2014. Reward processing by the lateral habenula in normal and depressive behaviors. Nature Publishing Group 17, 1146–1152. doi:10.1038/nn.3779
Quina, L.A., Tempest, L., Ng, L., Harris, J.A., Ferguson, S., Jhou, T.C., Turner, E.E., 2015. Efferent pathways of the mouse lateral habenula. The Journal of Comparative Neurology 523, 32–60. doi:10.1002/cne.23662
Roiser, J.P., Levy, J., Fromm, S.J., Nugent, A.C., Talagala, S.L., Hasler, G., Henn, F.A., Sahakian, B.J., Drevets, W.C., 2009. The Effects of Tryptophan Depletion on Neural Responses to Emotional Words in Remitted Depression. BPS 66, 441–450. doi:10.1016/j.biopsych.2009.05.002
Sartorius, A., Kiening, K.L., Kirsch, P., Gall, von, C.C., Haberkorn, U., Unterberg, A.W., Henn, F.A., Meyer-Lindenberg, A., 2010. Remission of Major Depression Under Deep Brain Stimulation of the Lateral Habenula in a Therapy-Refractory Patient. BPS 67, e9–e11. doi:10.1016/j.biopsych.2009.08.027
Schmidt, F.M., Schindler, S., Adamidis, M., Strauß, M., Tränkner, A., Trampel, R., Walter, M., Hegerl, U., Turner, R., Geyer, S., Schönknecht, P., 2016. Habenula volume increases with disease severity in unmedicated major depressive disorder as revealed by 7T MRI. European Archives of Psychiatry and Clinical Neuroscience 1–9. doi:10.1007/s00406-016-0675-8

Shabel, S.J., Proulx, C.D., Trias, A., Murphy, R.T., Malinow, R., 2012. Input to the Lateral Habenula from the Basal Ganglia Is Excitatory, Aversive, and Suppressed by Serotonin. Neuron 74, 475–481. doi:10.1016/j.neuron.2012.02.037

Sheehan, T.P., Chambers, R.A., Russell, D.S., 2004. Regulation of affect by the lateral septum: implications for neuropsychiatry. Brain Research Reviews 46, 71–117. doi:10.1016/j.brainresrev.2004.04.009

Shelton, L., Pendse, G., Maleki, N., Moulton, E.A., Lebel, A., Becerra, L., Borsook, D., 2012. Mapping pain activation and connectivity of the human habenula. Journal of Neurophysiology 107, 2633–2648. doi:10.1152/jn.00012.2012

Son, Y.-D., Cho, Z.-H., Choi, E.-J., Kim, J.-H., Kim, H.-K., Lee, S.-Y., Chi, J.-G., Park, C.-W., Kim, J.-H., Kim, Y.-B., 2014. Individually Differentiated Serotonergic Raphe Nuclei Measured with Brain PET/MR Imaging. Radiology 272, 541–548. doi:10.1148/radiol.14131547

Son, Y.-D., Cho, Z.-H., Kim, H.-K., Choi, E.-J., Lee, S.-Y., Chi, J.-G., Park, C.-W., Kim, Y.-B., 2012. Glucose metabolism of the midline nuclei raphe in the brainstem observed by PET–MRI fusion imaging. NeuroImage 59, 1094–1097. doi:10.1016/j.neuroimage.2011.09.036

Stephan, K.E., Tittgemeyer, M., Knösche, T.R., Moran, R.J., Friston, K.J., 2009. Tractography-based priors for dynamic causal models. NeuroImage 47, 1628–1638. doi:10.1016/j.neuroimage.2009.05.096

Strotmann, B., Heidemann, R.M., Anwander, A., Weiss, M., Trampel, R., Villringer, A., Turner, R., 2014. High-resolution MRI and diffusion-weighted imaging of the human habenula at 7 tesla. J. Magn. Reson. Imaging 39, 1018–1026. doi:10.1002/jmri.24252

Strotmann, B., Kögler, C., Bazin, P.-L., Weiss, M., Villringer, A., Turner, R., 2013. Mapping of the internal structure of human habenula with ex vivo MRI at 7T. Frontiers in Human Neuroscience 7, 878. doi:10.3389/fnhum.2013.00878

Sutherland, R.J., 1982. The Dorsal Diencephalic Conduction System: A Review of the Anatomy and Functions of the Habenular ComplexI. Neuroscience & Biobehavioral Reviews 6, 1–13.

Torrisi, S.J., O'Connell, K., Davis, A., Reynolds, R., Balderston, N., Fudge, J.L., Grillon, C., Ernst, M., 2015. Resting state connectivity of the bed nucleus of the stria terminalis at ultra-high field. Hum. Brain Mapp. 36, 4076–4088. doi:10.1002/hbm.22899

van der Zwaag, W., Francis, S., Head, K., Peters, A., Gowland, P., Morris, P., Bowtell, R., 2009. fMRI at 1.5, 3 and 7 T: Characterising BOLD signal changes. NeuroImage 47, 1425–1434. doi:10.1016/j.neuroimage.2009.05.015

Velasquez, K.M., Molfese, D.L., Salas, R., 2014. The role of the habenula in drug addiction. Frontiers in Human Neuroscience 8, 174. doi:10.3389/fnhum.2014.00174

Viswanath, H., Carter, A.Q., Baldwin, P.R., Molfese, D.L., Salas, R., 2013. The medial habenula: still neglected. Frontiers in Human Neuroscience 7, 931. doi:10.3389/fnhum.2013.00931

Yamaguchi, T., Danjo, T., Pastan, I., Hikida, T., Nakanishi, S., 2013. Distinct Roles of Segregated Transmission of the Septo-Habenular Pathway in Anxiety and Fear. Neuron 78, 537–544. doi:10.1016/j.neuron.2013.02.035

Zaborszky, L., Hoemke, L., Mohlberg, H., Schleicher, A., Amunts, K., Zilles, K., 2008. Stereotaxic probabilistic maps of the magnocellular cell groups in human basal forebrain. NeuroImage 42, 1127–1141. doi:10.1016/j.neuroimage.2008.05.055

Zhao, H., Zhang, B.-L., Yang, S.-J., Rusak, B., 2015. The role of lateral habenula–dorsal raphe nucleus circuits in higher brain functions and psychiatric illness. Behav. Brain Res. 277, 89–98. doi:10.1016/j.bbr.2014.09.016

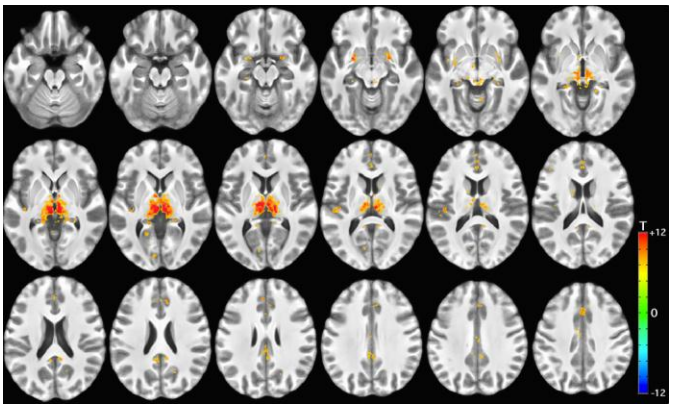
T
+12
0
-12

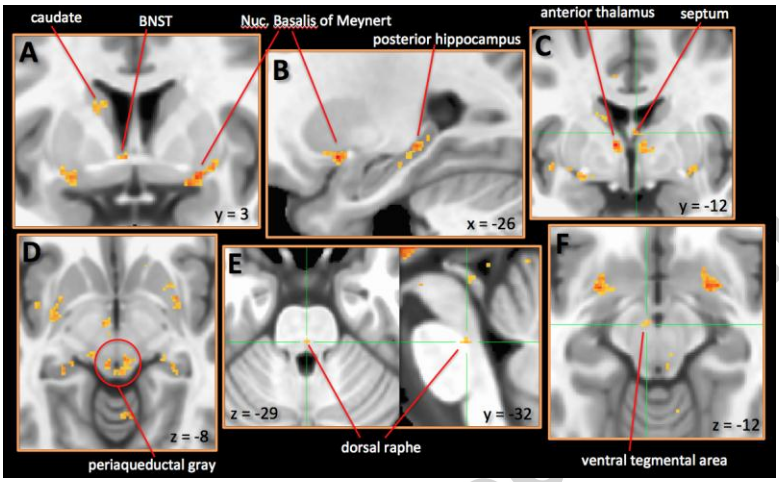
caudate
BNST
Nuc. Basalis of Meynert
posterior hippocampus
anterior thalamus
septum
A
B
C
y = 3
x = -26
y = -12
D
E
F
z = -8
z = -29
y = -32
z = -12
periaqueductal gray
dorsal raphe
ventral tegmental area

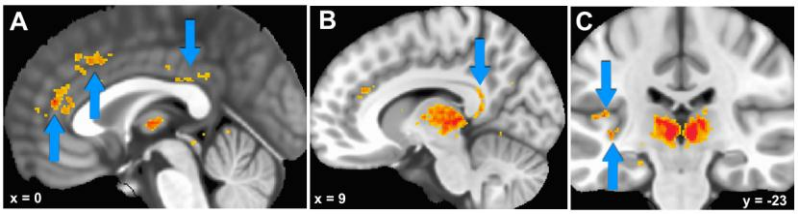
A
B
C
x = 0
x = 9
y = -23